Comparative Study on Properties of Nanocellulose Derived from Sustainable Biomass Resources

Zheng Cheng
South China University of Technology School of Light Industry and Engineering
Jinpeng Li
South China University of Technology School of Light Industry and Engineering
Bin Wang (febwang@scut.edu.cn)
South China University of Technology School of Light Industry and Engineering https://orcid.org/0000-0002-8114-7236
Jinsong Zeng
South China University of Technology School of Light Industry and Engineering
Jun Xu
South China University of Technology School of Light Industry and Engineering
Shiyun Zhu
South China University of Technology School of Light Industry and Engineering
Chengliang Duan
South China University of Technology
Kefu Chen
South China University of Technology School of Light Industry and Engineering

Research Article

Keywords: Nanocellulose, Cellulose nanocrystal, Cellulose nanofibril, Bacterial cellulose, Property comparison

Posted Date: May 9th, 2022

DOI: https://doi.org/10.21203/rs.3.rs-1344640/v1

Abstract

Nanocellulose, a unique and promising nanosized cellulose fibers extracted from renewable biomass, has gained much attention from both the scientific and industrial communities due to abundant resources, good mechanical properties, distinct surface chemistry, and biological properties. Thus, nanocellulose is a appealing biomaterial for exciting applications, including super absorbent materials, electronic components, energy devices, and reinforcements. Cellulose nanocrystal (CNC), cellulose nanofibril (CNF), and bacterial cellulose (BC) are the three kinds of typical nanocellulose from different routes, thus the comprehensive comparison of CNC, CNF, and BC is highly desirable. In order to better understand their special characteristics, we have described detailedly of CNC, CNF (including TEMPO oxidized CNF and mechanically ground CNF), and BC in current work. Meanwhile, this study systematically compared their preparation method, morphologies, chemical structure, surface chemistry, degree of polymerization, thermal behavior, mechanical property, and so on, all these are good for understanding the structure-property-function relationships of nanocellulose. The systematic comparative study can help to develop the criteria for selecting proper nanocellulose as biobased nanomaterials for high value-added applications. We believe that these detailed information presented here have the potential to achieve true sustainable, economic, and tailored production of nanocellulose at large scale, thus contributing to advancement of biobased nanocellulose.

Introduction

With increasing environmental and ecological issues caused by petroleum-based raw materials, the synthesis of target chemicals and multifunctional biomaterials from natural resources is of great utility value. Cellulose may prove to be one of the most promising sustainable biomaterials of modern times due to its intrinsic properties including abundance and renewability (Liu et al. 2021; Satam et al. 2018; Wang et al. 2020). Cellulose is an organic compound with the formula $(C_6H_{10}O_5)_n$, a polysaccharide consisting of a linear chain of repeated β(1→4) linked $_D$-glucose units, and abundant hydroxyl groups on the cellulose surface (French 2017; Kang et al. 2020; Nishiyama et al. 2002). Nanocellulose as a new form of biobased nanomaterials has been receiving an increasing amount of interest from both the scientific and industrial communities because of their interesting properties, including nanoscale size, fibril morphology, large surface area, and good strength (Abitbol et al. 2016; Chen et al. 2018; Zhao et al.). Nowadays, researches on nanocellulose-based materials are springing up like mushroom, which attracted a great concern in the field of high-performance materials and high technology (Cao et al. 2019; Cheng et al. 2021a). Thus, biomaterials based on nanocellulose become a hot division in the materials science (Duan et al. 2021). Normally, the nanocellulose can be divided into three types: cellulose nanocrystal (CNC), cellulose nanofibril (CNF), and bacterial cellulose (BC) (Thomas et al. 2018; Yang et al. 2015).

Generally, CNC and CNF are extracted from lignocellulosic biomass while bacterial cellulose (BC) is synthesized from certain kinds of bacteria using glucose by biosynthesis process (Foster et al. 2018; Guan et al. 2020). Regarding the common methods to prepare nanocellulose, CNC is normally produced from acid hydrolysis, and sulfuric acid as the conventional concentrated mineral acid is the most widely

used due to efficient selective hydrolysis of amorphous regions, but the environmental concerns about the corrosive nature and economic recovery of sulfuric acid remains beyond the reach of most applications (Giese et al. 2015; Habibi et al. 2010). CNF is mainly obtained from chemical, mechanical, or combinatorial processes. TEMPO-mediated oxidation coupled with mechanical treatment has become the mainstream approach to prepare CNF, which is ascribed to the fact that TEMPO-mediated oxidation is very effective in reducing fibrillation energy input (Chen et al. 2016; Isogai et al. 2011). However, the toxicity issues of TEMPO still needs to be addressed. Besides, BC could be conveniently generated from bacteria fermentation, but the incubation cycle takes time (Lin and Dufresne 2014; Yuan et al. 2020). Different preparation methods result in different properties of final nanocellulose products, which is of great importance for their practical application. Hence, it is very necessary to make a comprehensive study of the relationships between structure, property, and function of different types of nanocellulose, which can potentially guide for producing nanocellulose with tailored physicochemical properties.

As nanocellulose can be used to produce a variety of high-value products with low environmental and societal impact, and with growing public consciousness toward environmentally friendly and naturally sourced products, nanocellulose has already attracted both scientific and industrial attention and is destined for an important role in commercial society. Although there are many publications about the preparation method or application of nanocellulose, but studies about deep understanding and comparation of their structure-property relationships is less, and the uniqueness of each kind of nanocellulose is worth exploring for special use. Thus, this study systematically compared the origins, preparation method, morphologies, dimensions, chemical structure, surface chemistry, degree of polymerization, thermal behavior, and mechanical property of the CNC, CNF (including TEMPO oxidized CNF (TCNF) and mechanically ground CNF (MCNF)), and BC. The detailed comparative study is beneficial to develop the criteria for selecting proper nanocellulose as a green and sustainable nanosized biomaterial for high value-added applications.

Materials And Methods

Materials. The bleached softwood kraft pulp (BSKP) was homemade. Microcrystalline cellulose (MCC), TEMPO, NaBr, NaClO, and NaOH were purchased from Sigma-Aldrich Co. Ltd. Sulfuric acid (98 wt%) and regenerated cellulose dialysis tubes were purchased from Fisher Scientific. Acetobacter xylinum ATCC 23767 was obtained from Guangdong Microbial Culture Center (Guangzhou, China). All chemicals used in the preparation of culture media were obtained from Tianjin Benchmark Chemical Reagent Co., Ltd. (Tianjin, China). The water utilized throughout the experimental procedures was deionized (DI) water at room temperature.

Preparation of CNC. The CNC was prepared by controlled sulfuric acid hydrolysis of the microcrystalline cellulose, as described below (Gao et al. 2018). 10 g of microcrystalline cellulose was added to 100 ml of 64.0 wt % sulfuric acid under constant mechanical stirring. The hydrolysis was conducted at 45 ℃ and lasted for 50 minutes. The reaction was quenched by dilution with plenty of DI water, and the suspensions were washed with DI water by repeated centrifuging. The supernatant was removed from the

sediment and replaced with fresh deionized water and mixed. The centrifuge step was stopped until the supernatant became turbid. Subsequently, the resulting precipitate was dialyzed with deionized water for 14 days using regenerated cellulose dialysis membranes with a molecular weight cutoff of 12000–14000 until the water pH remained constant. Finally, the dialyzed suspension was centrifuged with the CNC remained in the supernatant. The samples were sonicated in an ice bath to avoid overheating, and then storage for further use.

Preparation of TEMPO Oxidized CNF. The TCNF was prepared by the TEMPO-mediated oxidation method. First, 2 g of dry weight BSKP was added to 100 mL of DI water containing 0.032 g of TEMPO, 0.2 g of NaBr, and 6 mL of 12.5 wt % NaClO solution (Sigma-Aldrich, USA), and the mixture was excellently dispersed using mechanical stirring. Then NaOH (0.5 mol/L) was added to maintain a pH = 10.5 at ambient temperature. After 2 h, the pH of the resulting mixture showed no further change, and the reaction was terminated. The oxidized cellulose fibers were sufficiently washed using DI water until the pH is 7.0, and the final product was named as TCNF (Saito et al. 2007).

Preparation of Mechanically Ground CNF. The BSKP fibers was immersed in deionized water at a concentration of 0.8 wt% for 2 h. Then the pulp suspensions were ground by super mass-colloider (MKCA6-2J, Masuko Sangyo Co. Ltd., Japan) at 2600 rpm. The gap between the two grinding stones was adjusted to -100 μm. The motion zero position was set as the contact position between two grinding stones before pulp suspension loading. At last, the suspensions were passed through the gap of + 50, +20, 0, -20, -50, -80 μm for 15 times, respectively. The CNF sample produced from mechanical grinding was marked as MCNF (Zeng et al. 2021).

Preparation of BC. The acetobacter xylinum (ATCC 23767) was cultured in a test tube for 2 day at 30 ℃ to increase the bacterial population. The suspension passed through multilayers of gauze. Then, the activated strain was then inoculated into a liquid culture medium of 6 v/v% capacity, fermented at 30 ℃ for several days (Cheng et al. 2017).

Preparation of Nanocellulose Films. The CNC film was prepared via 10 ml 3.0 wt % suspension casting in polypropylene Petri dishes at room temperature for at least 72 h. The TCNF film and MCNF film by pouring 0.3 wt % dispersion into the filter membrane with a 0.65 μm pore size, respectively. Wet nanopaper was fabricated by a filtration time of about 8.0 h and subsequently dried at 60 ℃ in a press. The BC film was obtained by pressing the BC aerogel (thickness: 20 cm) using of steel plate to thick flat film.

Transmission Electron Microscopy (TEM). The TEM images of all nanocellulose samples were obtained by using a JEM-1010 transmission electron microscopy (JEOL, Japan) at an accelerating voltage of 80 kV.

Scanning Electron Microscopy (SEM). The cross-section morphologies of the nanocellulose films were obtained by using a Scanning electron microscopy (SEM, S3700 Hitachi Ltd. Japan) at an accelerating voltage of 10 kV and the working distance was 11 mm.

Zeta Potential Test. The 0.1 wt % nanocellulose suspension was prepared, and the zeta potential of the suspension was measured at 25 ℃ using a zeta potential analyzer (HORIBA SZ-100, Japan). The reported zeta potential corresponded to the average value of five measurements.

Fourier Transform Infrared Spectroscopy (FTIR). The free-dried nanocellulose was deposited onto the KBr slice, and the FTIR spectra of the nanocellulose were recorded using a Nicolet FTIR 5700 spectrophotometer (Bruker, Germany) in transmission mode over the range of 500 to 4000 cm^{-1} with a 4 cm^{-1} resolution at 25 ℃.

Degree of Polymerization (DP). The average degree of polymerization was determined by viscosity (25°C) of nanocellulose solution in 0.5 mol/L cupriethylenediamine hydroxide solution using Ubbelohde viscometer. DP was determined from Eq. (1):

$$DP^{0.905} = 0.75[\eta]$$

1

The intrinsic viscosity [η] (cm^3/g) was calculated according to an ASTM method.

X-ray Diffraction (XRD). X-ray diffraction tests of four types of nanocellulose were conducted on an X-ray diffractometer (UI tima IV, Japan) using Cu kα radiation at 40 kV and 30 mA. The scan is from a two theta of 10°to 60°at a step size of 0.05°. A background correction was performed to collect data for a blank run and subtract if from the data on the samples.

The crystallinity index (CrI) was calculated from the following Eq. (2):

$$\mathrm{CrI}(\%) = (\mathrm{I}_{200} - \mathrm{I}_{\mathrm{am}}) / \mathrm{I}_{200} \times 100$$

2

Where I_{200} is the diffraction intensity of the (200) crystal lattice plane, which represents both crystalline and amorphous components, and I_{am} is the diffraction intensity of 2θ = 18°, representing the amorphous fraction (French and Cintrón 2013; Segal et al. 1959).

The average crystallite size (D_{hkl}) of the crystal in 200 lattice plane was determined by the Scherrer Eq. (3):

$D_{hkl} = \kappa\lambda/\beta\cos\theta$ (3)

Where, κ is the Scherrer constant (0.89), and λ is the wavelength of Cu-Ka radiation (0.15418 nm). β is the width of half height of the 200- lattice plane in radian, and θ is the Bragg's angle in radian when calculated in the excel spreadsheet (Wang et al. 2021).

Tensile Mechanical Test. The tensile mechanical properties of nanocellulose films (5 mm width × 25 mm length) were assessed by applying incremental tensional forces with an Instron model 5567 machine with crosshead speed control of 60 mm/min at room temperature.

Thermogravimetric Analysis (TGA). The thermal behavior of four types of nanocellulose samples were measured using SDTQ600 (TA Instruments, USA) under nitrogen atmosphere from 40 to 800°C at a heating rate of 10°C/ min.

Results And Discussion

As shown in Fig. 1, the production of CNC or CNF is a top-down procedure consisting in converting the large unit to the small unit (De France et al. 2020; Usov et al. 2015; Xu et al. 2013). In this study, the native cellulose (Fig. 1b) extracted from abundant trees (Fig. 1a) through mechanical and chemical treatment. The multiple hydroxyl groups on the cellulose from one chain to form hydrogen bonds with the same or a neighbor chain, holding the chains firmly together side-by-side. CNC is obtained through 64.0 wt % sulfuric acid hydrolysis and the amorphous regions of the cellulose microfibrils were selectively removed, thereby leaving crystalline nanorods (Fig. 1c) in the reaction solution. Besides, CNF is produced via TEMPO-mediated oxidation followed by mechanical fibrillation, or direct mechanical grinding treatment by super colloider (Fig. 1d). CNFs form long fiber with a fibril diameter similar to or larger than CNCs, and the length vary from several hundreds of nanometers to micrometers. CNF contains amorphous area and are not as highly crystalline as CNC (Dias et al. 2020). Contrary to the production of CNC and CNF, the biosynthesis of BC is a bottom-up process of construction from tiny unit to small unit. BC is typically generated by a acetobacter xylinum fermentation process (Fig. 1e, f), and the synthesis is a hierarchical process. BC does not contain lignin, hemicellulose or other non-degradable molecules, and hence much purer (Cheng et al. 2021b).

Straightforward characteristics of nanocellulose are their external forms and morphologies, giving us the most direct impression. Therefore, the general appearance of nanocellulose is shown in Fig. 2, and their final form is generally an aqueous suspension or gel after just produced. After sulfuric acid hydrolysis to produce CNC, they are diluted with water and purified, giving a suspension with different concentrations. Figure 2a shows 1.0 wt % CNC suspension which is transparent with a translucent blueish hue, and negatively charged CNCs can form stable colloidal suspensions at this low concentrations. A hydrogel will form when increased the concentration to about 10.0 wt% (Fig. 2b). And a white powder form will be obtained after the CNC suspension goes through a freeze-drying process (Fig. 2c). In comparison, the TEMPO oxidized CNFs form a gel at low concentrations of 2.0 wt% (Fig. 2d), and are a thick paste by 10.0 wt% (Fig. 2e). The freeze dried forms of TCNF can be also obtained at high concentration (Fig. 2f), while it can not be redispersed back to individual nanofibrils. As comparison to TCNF, the MCNF with low concentrations are very similar in appearance and properties (Fig. 2g), MCNF can show a much larger range of dimensions in the mixture. The MCNF could form paste with suspensions concentrations as low as 2.0 wt% (Fig. 2h), and the dense paste is obtained after increased the concentration to 10.0 wt% (Fig. 2i). This can be explained by the fact that low charges and lots of hydrogen bonds on MCNF, leading

to more aggregation among MCNF fibers. Unlike CNC and CNF, BC is a state of pellicle with various thickness. Figure 2j, k are 3 mm and 15 mm, respectively, and a foam-like aerogel will form after freeze drying (Fig. 2i).

The morphology and dimensions of nanocellulose can be studied with TEM images. As seen from Fig. 3, both size and aspect ratio depend strongly on the cellulose source and the processing technique, and each source/process yields the nanocellulose with distinct characteristics. Sulfuric acid hydrolysis of cellulose pulp produces short rod-like CNCs with an average diameter of 5–60 nm and length of 100–300 nm (Fig. 3a). It is apparent that the fine CNC nanoparticles have uniform dispersion, and no obvious aggregation of individual nanocrystals. TEMPO-mediated oxidation of pulp yields extremely thin nanofibers with an average length from of several hundred nanometers to micrometers (Fig. 3b). While the mechanically ground CNFs with no added chemicals yields the larger nanofibers (both diameter and length) than TCNFs, within the diameter of 5–300 nm and length from nano-scale to micron-scale (Fig. 3c). The BC exhibits a porous, interconnected, and ultrafine 3D nanofibrillar reticulated structure (Fig. 3d), and the nanofibers with a diameter of 30–80 nm and the length ranging from 200 nm to several μm. The highly entangled structure of BC significantly increases resistance to flow and results in gel-like behavior of the BC sample. Given BC's complex network morphology, it was difficult to measure the length and diameter of individual BC nanofiber with high accuracy (Jiang et al. 2019). Indeed, the range of morphologies and dimensions observed for four types of nanocellulose by simply varying the technical process, reveals the tunability of nanocellulose preparation. It is also true that some of the variation in morphology and size could be from the different sources. These could act as a tool to guide decision-making for selection of methods to produce nanocellulose with tailored dimensions.

It is known that the easy aggregation of nanocellulose is a common problem. So far, technologies for dispersing nanocellulose have been studied in various ways (Frank et al. 2018; Kedzior et al. 2021). Thus, techniques for modifying the surface of nanocellulose are to impart functional groups to nanocellulose (Afrin and Karim 2017; Fatona et al. 2018). The chemical structures present on the various nanocellulose are shown in Fig. 4. Since the CNCs are produced via sulfuric acid hydrolysis procedure, and the sulfuric acid as hydrolyzing agents could react with the surface hydroxyl groups of cellulose to yield negatively charged surfaces bearing sulfate esters ($-OSO_3^-$) (Cheng et al. 2019), which promote a spontaneous dispersion of CNCs in water (Fig. 4a). The chemical structures of TCNF is presented in Fig. 4b. Oxidation mediated by TEMPO can be used as a method to promote nanocellulose separation, and the C6 primary hydroxyls of cellulose can be entirely and selectively converted to C6 sodium carboxylate groups (-COOH) (Camargos and Rezende 2021). Meanwhile, a high degree of charge is obtained due to the introduction of anionic carboxylates, thus resulting in better dispersibility in water. The negative charges on the TCNF surface introduced via this oxidation technique could increase the electrostatic repulsive forces. However, there is no other functional groups except hydroxyl groups on the cellulose chains for MCNF and BC, leaving the surface chemistry of the nanocellulose unchanged (Fig. 4c). Because no chemical reaction is occurred to obtain MCNF, and the BC is pure cellulose composed of vast nanofibrils.

The colloidal stability of nanocellulose is often the result of electrostatic repulsion due to the presence of charged groups at the particle surface. Generally, suspensions with absolute zeta potential values above 30 mV are considered colloidally stable (Raphael et al. 2014). In the study, the zeta potentials of three typical nanocellulose are shown in Fig. 5a. It can be seen that the sulfuric acid hydrolyzed CNC with a zeta potential of -37.1 mV due to the $-OSO_3^-$ groups derived from esterification of the hydroxyl groups, and the TEMPO oxidized CNFs has a highly negative potential up to -63.8 mV due to the oxidation hydroxyl groups to carboxylic group in the C6 position. The mechanically ground CNF with a zeta potential of -16.2 mV because of no functional groups. In addition, the BC has a weak negative charge caused by the hydroxyl groups of cellulose, and hence the value for BC is just − 11.5 mV. The crystallinity of the three kinds of nanocellulose were investigated using X-ray diffraction (XRD), as shown in Fig. 5b. The results indicate that the crystallinity of CNC samples from sulfuric acid hydrolysis was 81.65%, which is higher than CNF samples from TEMPO oxidation with 62.48%. The increase in crystallinity of CNC was a result of hydrolysis of hemicellulose and disordered cellulose of the native fibers. In addition, the MCNF with the crystallinity of 68.92%, producing a higher value for TCNF and a lower value for CNCs. This is because that CNFs have both a crystalline and an amorphous region (Chen et al. 2021; Thomas et al. 2018). Each microfibril consists of a crystalline domain intermixed with disordered amorphous regions. It is worth noting that BC displays a distinct crystallinity of up to 88.73%, which can be explained by the fact that BC does not contain lignin, hemicellulose or other non-degradable molecules and it is with high purity. In addition, the average crystallite size (D_{hkl}) of the crystal in 200 lattice plane of CNC, TCNF, MCNF, and BC was about 3.10 nm, 3.25 nm, 3.52 nm, and 3.64 nm respectively. We could find that the Segal crystallinity increased with the crystallite size increased, showing a positive correlation.

At the molecular scale, cellulose biopolymers have a linear chain structure consisting of $_D$-glucose unit via β (1–4) linkage with a degree of polymerization. Thus, DP of nanocellulose could reflects the number of glucopyranose in each cellulose molecule, which acts as a measure of the length of nanocellulose chains. Meanwhile, DP can reflect the level of cellulose chains degradation (Fang et al. 2020). Generally speaking, chemical and mechanical treatments all result in the degradation of cellulose, and the more severe treatment lead to more severe DP reduction. As shown in Fig. 5c, acid hydrolysis, TEMPO oxidation, and grinding all reduced the DP of cellulose fiber significantly. Among them, the BC had the maximum DP value of 2862, indicating high degree of polymerization and high purity. The original BSKP with DP value of 782, and the grinding process had the minimal impact on DP reduction because pure mechanical treatment could not destroy the construction of fibers completely and still retained many original fibers, thus MCNF possesses DP value of 473. Meanwhile, more intense TEMPO oxidation treatments also caused the DP of BSKP to drop further, and the DP of TCNF was reduced by 40.60% compared with MCNF. In addition, acid hydrolysis resulted in the most severe DP degradation and reduced the DP of MCC fibers from 140 to 65. The FTIR spectra were used to investigate the chemical composition of nanocellulose. As shown in Fig. 5d, the FTIR spectrum of the CNC, TCNF, MCNF, and BC showed several similar peaks of functional groups, such as C-O, C-H, $-CH_2$, and -OH. Typically, the peaks at 3340 cm^{-1} and 1048 cm^{-1} are attributed to the -OH stretching vibration and the C-O bond of native cellulose, respectively. And the peaks at 2900 cm^{-1} and 1426 cm^{-1} corresponds to the C-H stretching and

bending of the -CH_2 groups, respectively (Wang et al. 2017). Furthermore, the peak at 1640 cm^{-1} is assigned to the -OH stretching vibration of absorbed water (H_2O). The MCNF and BC show similar FTIR spectra to the original cellulose. Importantly, the peak at 1730 cm^{-1} in TCNF confirms the presence of carboxylic acid groups, and the peak at 1205 cm^{-1} in CNC related to S = O vibration due to the esterification (Lu and Hsieh 2010; Neto et al. 2013).

The solid CNC films exhibit iridescent color originated from the inside periodic layered structure formed after certain concentration of nanocrystals suspension via evaporation (Fig. 6a). It is observed that the long-range helical order is evident throughout the entire thickness, and the periodic layered structure is uniform and well-organized. The biosourced photonic film is appealing to both academia and industries, where optical and photonic components are essential. CNC film iridescence color has been promoted as a mean to provide color benignly in consumer products, to develop authenticating devices in security paper and to make UV and IR reflective barriers (Fernandes et al. 2017; Zheng et al. 2018). The TCNF film with high transparency and good mechanical flexibility has been named “nanopaper”, and looks like a thin plastic film to the naked eye (Fig. 6b). This TCNF film possesses a dense structure. The transparent nanopaper with optimal transmittance and surface smoothness enable a wide range of interesting applications such as renewable and clean “green” electronics wearable including systems for personal health monitoring and smart gloves with integrated sensors (Jung et al. 2015). Besides, another type of film made from MCNF, exhibiting low opacity due to rough and disorderly structure, thus the light could not easily pass through it (Fig. 6c). A super BC film is obtained by hot press process (Fig. 6d). The BC film has fibrous structure owing to the alignment of nanofibers, and the porous network structure gives the BC film excellent flexibility and can be used as promising building blocks for future high-performance biomaterials and textiles (Wang et al. 2018).

The tensile strength and modulus test was performed to study the mechanical properties of the four kinds of nanocellulose films, as shown in Fig. 7a, b. Among these nanocellulose films, BC films exhibited the highest strength up to 147.62 MPa and lowest Young’s modulus of 2.61 GPa, which is due to the strong hydrogen bonding and large aspect ratio (Wang et al. 2018). However, the CNC film with the lowest tensile strength of 21.38 MPa and highest Young’s modulus of 5.73 GPa, showing a typical brittle characteristic. Moreover, the tensile strength of TCNF film (109.87 MPa) is superior to MCNF film (72.68 MPa) because of the abundant hydrogen bonds originated from carboxyl and hydroxyl groups among TCNF (Guan et al. 2021). Meanwhile, the weaker bonding force of MCNF resulting in a lower Young’s modulus than TCNF film. Thus, the average Young’s modulus of TCNF film and MCNF film was 5.18 GPa, 4.20 GPa, respectively. In brief, the mechanical properties of nanocellulose films could be affected by their source, size dimensions, aspect ratio, and surface functional groups. The thermal stabilities of nanocellulose were determined to assess its potential use in high-temperature applications. The thermogravimetric (TG) and derivative thermogravimetric (DTG) curves of these four types of nanocellulose are illustrated in Fig. 7c, d. The TG curves showed a small weight loss before 150 °C, corresponding to moisture evaporation. Among the samples, CNC exhibited the lowest thermal stability due to the disruption of its crystalline structure and introduction of sulfate groups during sulfuric acid

hydrolysis. In addition, small fiber size dimensions exhibit high specific surface areas, thus more sites exposed to heat also could lower the thermal stability (Park et al. 2019). Furthermore, TCNF exhibited lower thermal stability than MCNF, but higher than CNC. MCNF showed slightly lower thermal stability than the BC. On the other hand, CNC exhibited approximate yield (26.0%) of char residues with TCNF and BC, while higher yield than MCNF (22.7%). The increased char residues might be due to the dehydration reaction at lower temperatures. The CNC and TCNF sample exhibited double degradation peaks, possibly because of its wide size distribution and different degrees of esterification and oxidation.

A comparison of the physical properties, preparation processes, and life-cycle assessments of these four kinds of nanocellulose are summarized in Table 1. Overall, the mechanical method to prepare MCNF is eco-friendly and simple, but needs high energy consumption as well as wide particle size distribution and low crystallinity of product. Acid hydrolysis preparation of CNC is mature, and the CNC particle size distribution is narrow, but the reaction equipment must be able to resist the corrosion of strong acid, and waste acids produced must be treated. Chemical agent such as TEMPO used to prepare TCNF is facile and could obtain narrow size distribution product, while the process is toxic and corrosive. Bacterial biosynthesis methods are green, with low energy consumption, no pollution, and mild production conditions, but their production efficiency is low and they have a long production cycle. In general, there are many ways to prepare nanocellulose, but each method has limitations (Zhu et al. 2016). In fact, nanocellulose production often combines several methods to use their advantages and avoid their shortcomings (Chen et al. 2018). At present, combinations of chemical and mechanical methods have become mainstream.

Table 1
Comparison of the physical properties, process, and life-cycle assessments of nanocellulose

Type	CNC	TCNF	MCNF	BC
Source	Microcrystalline cellulose	Bleached softwood kraft pulp	Bleached softwood kraft pulp	Biosynthesis by bacteria
Diameter	5–60 nm	5-100 nm	5-300 nm	30–80 nm
Length	100–300 nm	Nano-microns	Nano-microns	Nano-microns
Size distribution	Polydisperse	Polydisperse	Polydisperse	Aggregation
Conductivity	None	None	None	None
Optical properties	Iridescent films	Transparent films	Transparent films	Transparent films
Process	Waste acid	Waste alkali	Green	Green
Energy consumption	Moderate	Moderate	High	Low
Cost	High	Moderate	High	Low
Yield	38.7%	46.5%	75.3%	41.8%
Major application	Coatings, adhesives, food, paints	Packaging, transparent film, nanocomposites	Drug delivery, cosmetics, reinforcer,	Biomedical implants, wound dressings
Ecotoxicity	Low toxicity	Low toxicity	Low toxicity	Low toxicity
Disposal	Biodegradable	Biodegradable	Biodegradable	Biodegradable

Conclusions

A systematic comparison between CNC, CNF, and BC is made in this study with focus on their origins, preparation method, morphologies, dimensions, solid membrane, chemical structure, surface chemistry, degree of polymerization, thermal behavior, and mechanical property. Several kinds of measurement methods (TEM, SEM, Zeta potential, XRD, FTIR, TGA, DP, and tensile test) were used to gather and compare structural and chemical information on the these four typical nanocellulose. The information gathered here affords a direct comparison of the key properties of the nanocellulose. We provide our perspective from structure-property-function relationships to understand the nanocellulose and the results from this comparative study are important for proper selection of nanocellulose as advanced functional biomaterials, and thus promote the opportunities for industrialization. Generally speaking, although there have been many promising achievements in the laboratory, several challenges achieving industrial-scale, low-cost, and eco-friendly production of nanocellulose still remain. Furthermore, process optimization

targeting improved preparation methods is urgently required. Besides, certain surface modification for the end uses of nanocellulose-based products are needed.

Declarations

Acknowledgments

The research is supported by National Natural Science Foundation of China (22108086 & 22078113), Guangdong Basic and Applied Basic Research Foundation (2019A1515010996 & 2020A1515110855 & 2022A1515010323), Science and Technology Planning Project of Guangzhou (202102020891 & 202102080416 & 202102020713), Guangdong Provincial Key Laboratory of Plant Resources Biorefinery (2021B1212040011), Characterization and Instrument Development of Cross-scale Nanofiber Based on Microfluidic Technology (2020ZD01), the Foundation (No. GZKF202022) of State Key Laboratory of Biobased Material and Green Papermaking, Qilu University of Technology, Shandong Academy of Sciences. We are grateful for these financial support.

Conflict of interest

The authors declare no conflict of interest.

References

1. Abitbol T et al (2016) Nanocellulose, a tiny fiber with huge applications. Curr Opin Biotechnol 39:76–88
2. Afrin S, Karim Z (2017) Isolation and Surface Modification of Nanocellulose: Necessity of Enzymes over. Chemicals ChemBioEng Reviews 4:289–303. doi:https://doi.org/10.1002/cben.201600001
3. Camargos CHM, Rezende CA (2021) Structure–Property Relationships of Cellulose Nanocrystals and Nanofibrils: Implications for the Design and Performance of Nanocomposites and All-Nanocellulose Systems. ACS Appl Nano Mater 4:10505–10518. doi:10.1021/acsanm.1c02008
4. Cao D et al (2019) 3D Printed High-Performance Lithium Metal Microbatteries Enabled by Nanocellulose Advanced Materials:1807313
5. Chen L, Zhu J, Baez C, Kitin P, Elder T (2016) Highly thermal-stable and functional cellulose nanocrystals and nanofibrils produced using fully recyclable organic acids. Green Chem 18:3835–3843
6. Chen S, Zhang Z-L, Song F, Wang X-L, Wang Y-Z (2021) Rapid Synthesis of Polymer-Grafted Cellulose Nanofiber Nanocomposite via Surface-Initiated Cu(0)-Mediated Reversible Deactivation. Radical Polymerization Macromolecules 54:7409–7420. doi:10.1021/acs.macromol.1c00903
7. Chen W, Yu H, Lee S-Y, Wei T, Li J, Fan Z (2018) Nanocellulose: a promising nanomaterial for advanced electrochemical energy storage. Chem Soc Rev 47:2837–2872. doi:10.1039/C7CS00790F

8. Cheng R et al (2021a) Ultralight, flexible and conductive silver nanowire/nanofibrillated cellulose aerogel for multifunctional strain sensor. Chem Eng J 424:130565. doi:https://doi.org/10.1016/j.cej.2021.130565
9. Cheng Z et al (2021b) Bottom-Up Ecofriendly Strategy for Construction of Sustainable Bacterial Cellulose Bioaerogel with Multifunctional Properties. Adv Mater Interfaces 8:2002101. doi:https://doi.org/10.1002/admi.202002101
10. Cheng Z et al (2019) Plasmonic-Enhanced Cholesteric Films: Coassembling Anisotropic Gold Nanorods with Cellulose. Nanocrystals Adv Opt Mater 7:1801816. doi:https://doi.org/10.1002/adom.201801816
11. Cheng Z, Yang R, Liu X, Liu X, Chen H (2017) Green synthesis of bacterial cellulose via acetic acid pre-hydrolysis liquor of agricultural corn stalk used as carbon source. Bioresour Technol 234:8–14
12. De France K, Zeng Z, Wu T, Nyström G (2020) Functional Materials from Nanocellulose: Utilizing Structure-Property Relationships in Bottom-Up. Fabrication Adv Materials:2000657. doi:10.1002/adma.202000657
13. Dias O, Konar S, Leao A, Yang W, Tjong J, Sain M (2020) Current State of Applications of Nanocellulose in Flexible Energy and Electronic Devices. Front Chem 8:420. doi:10.3389/fchem.2020.00420
14. Duan C et al (2021) Chiral Photonic Liquid Crystal Films Derived from. Cellulose Nanocrystals Small 17:2007306. doi:https://doi.org/10.1002/smll.202007306
15. Fang Z et al (2020) Critical Role of Degree of Polymerization of Cellulose in Super-Strong. Nanocellulose Films Matter 2:1000–1014. doi:https://doi.org/10.1016/j.matt.2020.01.016
16. Fatona A, Berry RM, Brook MA, Moran-Mirabal JM (2018) Versatile Surface Modification of Cellulose Fibers and Cellulose Nanocrystals through Modular Triazinyl. Chem Chem Mater 30:2424–2435. doi:10.1021/acs.chemmater.8b00511
17. Fernandes SN et al (2017) Mind the microgap in iridescent cellulose nanocrystal films. Adv Mater 29:1603560
18. Foster EJ et al (2018) Current characterization methods for cellulose nanomaterials. Chem Soc Rev 47:2609–2679
19. Frank BP et al (2018) Impact of Silanization on the Structure, Dispersion Properties, and Biodegradability of Nanocellulose as a Nanocomposite Filler. ACS Appl Nano Mater 1:7025–7038. doi:10.1021/acsanm.8b01819
20. French AD (2017) Glucose, not cellobiose, is the repeating unit of cellulose and why that. is important Cellulose 24:4605–4609. doi:10.1007/s10570-017-1450-3
21. French AD, Cintrón MS (2013) Cellulose polymorphy, crystallite size, and the Segal. Crystallinity Index Cellulose 20:583–588
22. Gao Y, Xu H, Cheng Q (2018) Multiple Synergistic Toughening Graphene Nanocomposites through Cadmium Ions and Cellulose Nanocrystals Advanced Materials Interfaces:1800145

23. Giese M, Blusch LK, Khan MK, MacLachlan MJ (2015) Functional Materials from Cellulose-Derived Liquid-Crystal. Templates Angewandte Chemie International Edition 54:2888–2910
24. Guan Q-F, Yang H-B, Han Z-M, Ling Z-C, Yang K-P, Yin C-H, Yu S-H (2021) Plant Cellulose Nanofiber-Derived Structural Material with High-Density Reversible Interaction Networks for Plastic Substitute Nano Letters. 10.1021/acs.nanolett.1c02315
25. Guan Q-F et al (2020) Lightweight, tough, and sustainable cellulose nanofiber-derived bulk structural materials with low thermal expansion coefficient. Sci Adv 6:eaaz1114. doi:10.1126/sciadv.aaz1114
26. Habibi Y, Lucia LA, Rojas OJ (2010) Cellulose nanocrystals: chemistry, self-assembly. Appl Chem reviews 110:3479–3500
27. Isogai A, Saito T, Fukuzumi H (2011) TEMPO-oxidized cellulose nanofibers nanoscale 3:71–85
28. Jiang J, Zhu J, Zhang Q, Zhan X, Chen F (2019) A Shape Recovery Zwitterionic Bacterial Cellulose Aerogel with Superior Performances for. Water Remediation Langmuir 35:11959–11967. doi:10.1021/acs.langmuir.8b04180
29. Jung YH et al (2015) High-performance green flexible electronics based on biodegradable cellulose nanofibril paper. Nat Commun 6:7170
30. Kang L et al (2020) Degradable dual superlyophobic lignocellulosic fibers for high-efficiency oil/water separation. Green Chem 22:504–512. doi:10.1039/C9GC03861B
31. Kedzior SA, Gabriel VA, Dubé MA, Cranston ED (2021) Nanocellulose in Emulsions and Heterogeneous Water-Based Polymer Systems. Rev Adv Mater 33:2002404. doi:https://doi.org/10.1002/adma.202002404
32. Lin N, Dufresne A (2014) Nanocellulose in biomedicine: Current status and future prospect. Eur Polymer J 59:302–325
33. Liu C et al (2021) Biopolymers Derived from Trees as Sustainable Multifunctional Materials. Rev Adv Mater 33:2001654. doi:https://doi.org/10.1002/adma.202001654
34. Lu P, Hsieh Y-L (2010) Preparation and properties of cellulose nanocrystals: rods, spheres, and network. Carbohydr Polym 82:329–336
35. Neto WPF, Silvério HA, Dantas NO, Pasquini D (2013) Extraction and characterization of cellulose nanocrystals from agro-industrial residue–Soy. hulls Industrial Crops and Products 42:480–488
36. Nishiyama Y, Langan P, Chanzy H (2002) Crystal structure and hydrogen-bonding system in cellulose Iβ from synchrotron X-ray and neutron fiber diffraction. J Am Chem Soc 124:9074–9082
37. Park Y et al (2019) Thermal conductivity enhancement in electrospun poly(vinyl alcohol) and poly(vinyl alcohol)/cellulose nanocrystal composite nanofibers. Sci Rep 9:3026. doi:10.1038/s41598-019-39825-8
38. Raphael B, Naceur B, Julien B (2014) Flexibility and Color Monitoring of Cellulose Nanocrystal Iridescent Solid Films Using Anionic or Neutral. Polymers Acs Applied Materials & Interfaces
39. Sacui IA et al (2014) Comparison of the properties of cellulose nanocrystals and cellulose nanofibrils isolated from bacteria, tunicate, and wood processed using acid, enzymatic, mechanical, and

oxidative methods. ACS Appl Mater Interfaces 6:6127–6138

40. Saito T, Kimura S, Nishiyama Y, Isogai A (2007) Cellulose nanofibers prepared by TEMPO-mediated oxidation of. native cellulose Biomacromolecules 8:2485–2491
41. Satam CC, Irvin CW, Lang AW, Jallorina JCR, Shofner ML, Reynolds JR, Meredith JC (2018) Spray-Coated Multilayer Cellulose Nanocrystal—Chitin Nanofiber Films for Barrier Applications. ACS Sustain Chem Eng 6:10637–10644. doi:10.1021/acssuschemeng.8b01536
42. Segal L, Creely JJ, Martin AE, Conrad CM (1959) An Empirical Method for Estimating the Degree of Crystallinity of Native Cellulose Using the X-Ray Diffractometer. Text Res J 29:786–794. doi:10.1177/004051755902901003
43. Thomas B et al (2018) Nanocellulose, a Versatile Green Platform: From Biosources to Materials and Their Applications Chemical Reviews 118 doi:10.1021/acs.chemrev.7b00627
44. Usov I et al (2015) Understanding nanocellulose chirality and structure–properties relationship at the single fibril level. Nat Commun 6:7564
45. Wang M, Shao C, Zhou S, Yang J, Xu F (2017) Preparation of carbon aerogels from TEMPO-oxidized cellulose nanofibers for organic solvents absorption. RSC Adv 7:38220–38230
46. Wang P, Huang L, He L, Gao W, Wang Z (2021) Characteristics of Concentrated Lignocellulosic Nanofibrils Suspension Cellulose 29:147–158
47. Wang S et al (2018) Transparent, anisotropic biofilm with aligned bacterial cellulose nanofibersAdvanced Functional Materials:1707491
48. Wang X et al (2020) All-Natural, Degradable, Rolled-Up Straws Based on Cellulose Micro- and Nano-Hybrid. Fibers Adv Funct Mater. doi:10.1002/adfm.201910417
49. Xu X, Liu F, Jiang L, Zhu J, Haagenson D, Wiesenborn DP (2013) Cellulose nanocrystals vs. cellulose nanofibrils: a comparative study on their microstructures and effects as polymer reinforcing agents. ACS Appl Mater Interfaces 5:2999–3009
50. Yang X, Shi K, Zhitomirsky I, Cranston ED (2015) Cellulose nanocrystal aerogels as universal 3D lightweight substrates for supercapacitor materials. Adv Mater 27:6104–6109
51. Yuan H, Chen L, Hong FF, Healing (2020)ACS Applied Materials & Interfaces12:3382–3392doi:10.1021/acsami.9b17732
52. Zeng J, Zeng Z, Cheng Z, Wang Y, Wang X, Wang B, Gao W (2021) Cellulose nanofibrils manufactured by various methods with application as paper strength additives Scientific Reports. 11. 10.1038/s41598-021-91420-y
53. Zhao D, Zhu Y, Cheng W, Chen W, Wu Y, Yu H, Cellulose-BasedFlexible Functional Materials for Emerging Intelligent Electronics Advanced Materials n/a:2000619doi:10.1002/adma.202000619
54. Zheng H, Li W, Li W, Wang X, Tang Z, Zhang SXA, Xu Y (2018) Uncovering the Circular Polarization Potential of Chiral Photonic Cellulose Films for. Photonic Appl Adv Mater 30:1705948
55. Zhu H et al (2016) Wood-Derived Materials for Green Electronics, Biological Devices, and Energy Applications Chemical Reviews 116:9305–9374 doi:10.1021/acs.chemrev.6b00225

Figures

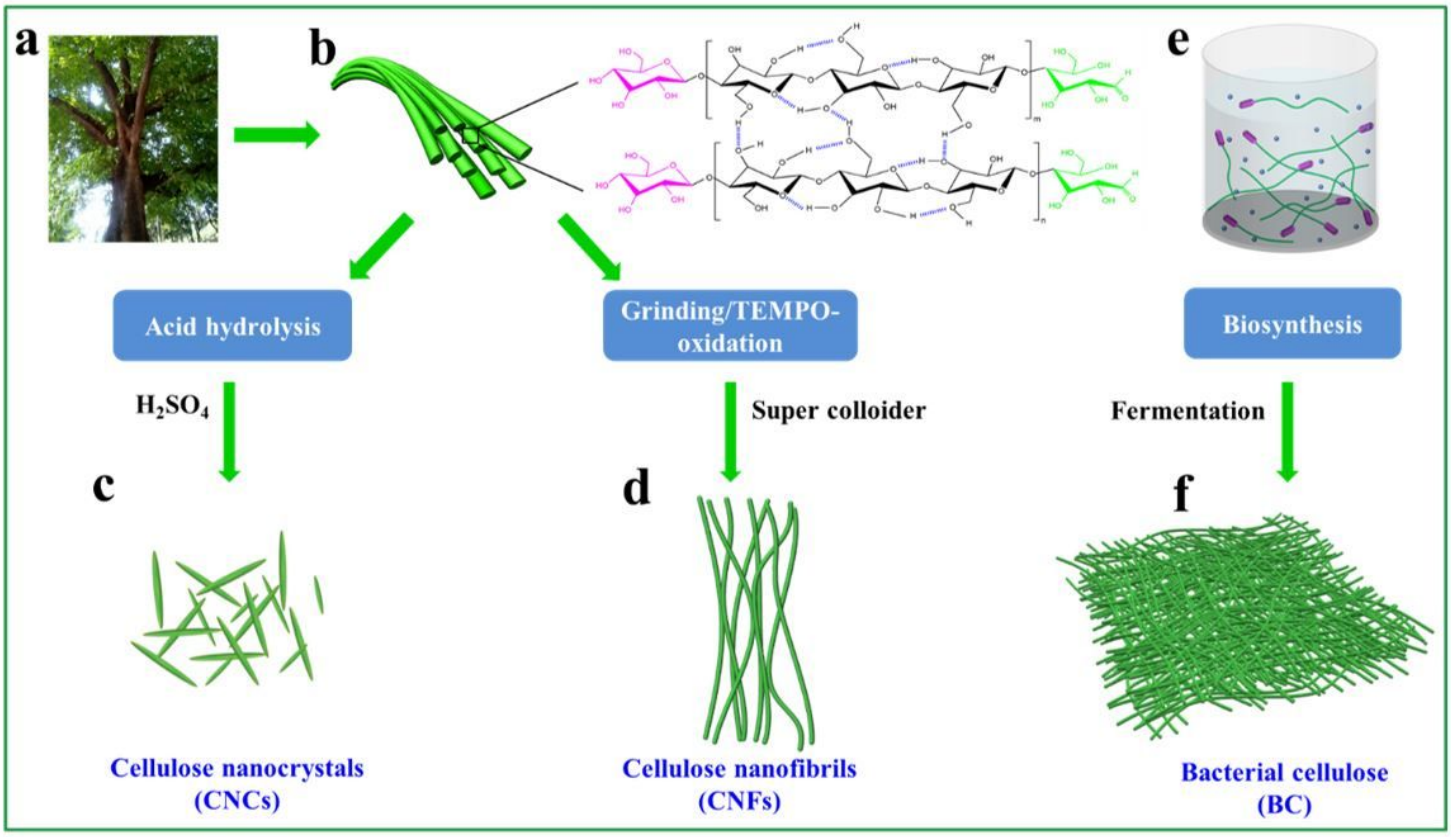

Figure 1

Schematic illustration of the preparation and synthesis process of nanocellulose. (a) Green tree, (b) Wood fiber, (c) CNC suspension, (d) CNF suspension, (e) Acetobacter xylinum under static cultivation condition to produce bacterial cellulose, (f) BC pellicle

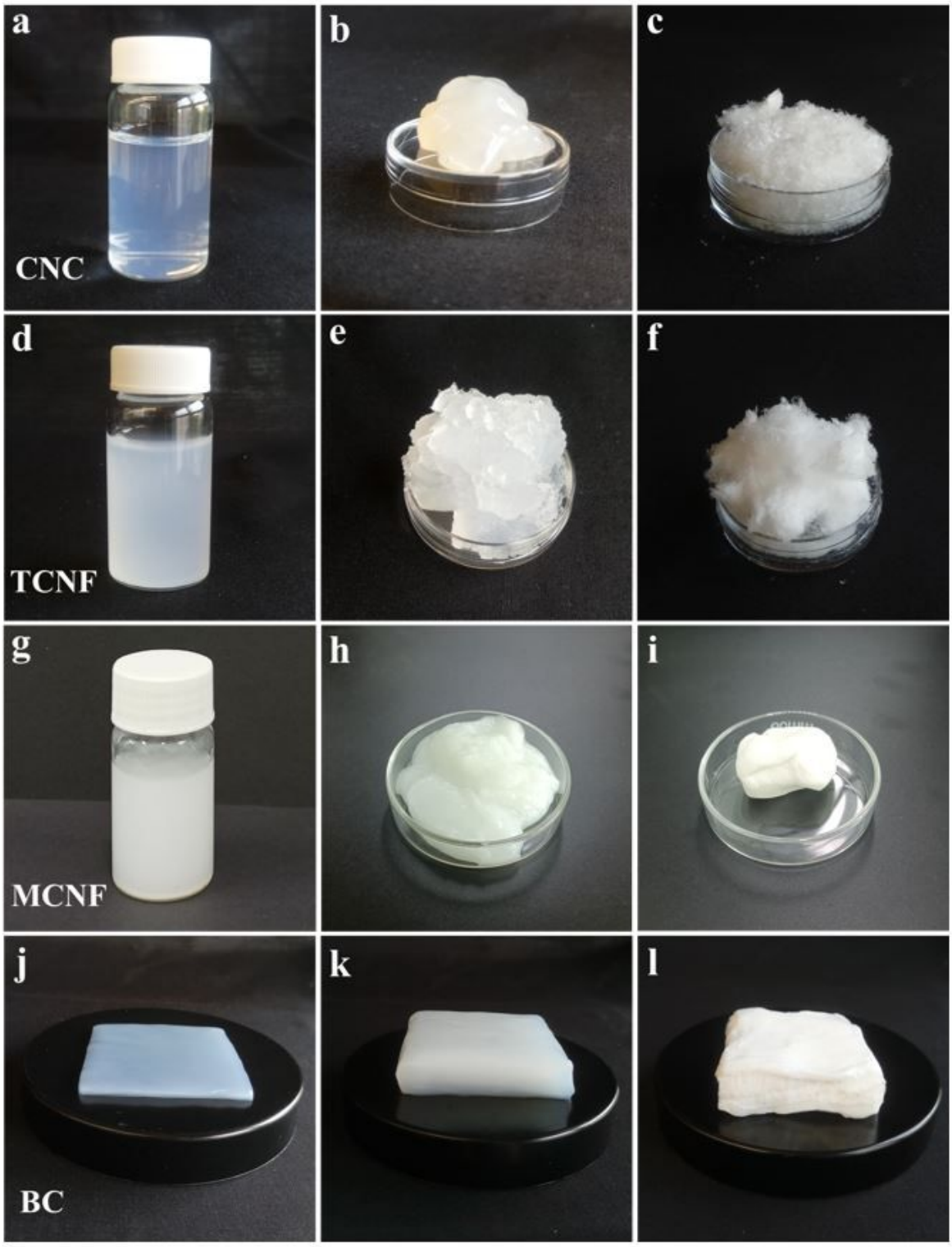

Figure 2

Photographs of nanocellulose, showing sulfuric acid hydrolyzed CNCs in the top row, TCNF and MCNF in the middle rows, and BC in the bottom row. (a) 1.0 wt% CNC suspension, (b) 10.0 wt% CNC hydrogel, (c) Freeze dried CNC, (d) 2.0 wt% TCNF suspension, (e) 10.0 wt% TCNF hydrogel, (f) Freeze dried TCNF, (g) 0.6 wt% MCNF suspension, (h) 2.0 wt% MCNF hydrogel, (i) 10.0 wt% MCNF paste, (j) 3 mm BC hydrogel, (k) 15 mm BC hydrogel, (l) freeze dried BC aerogel

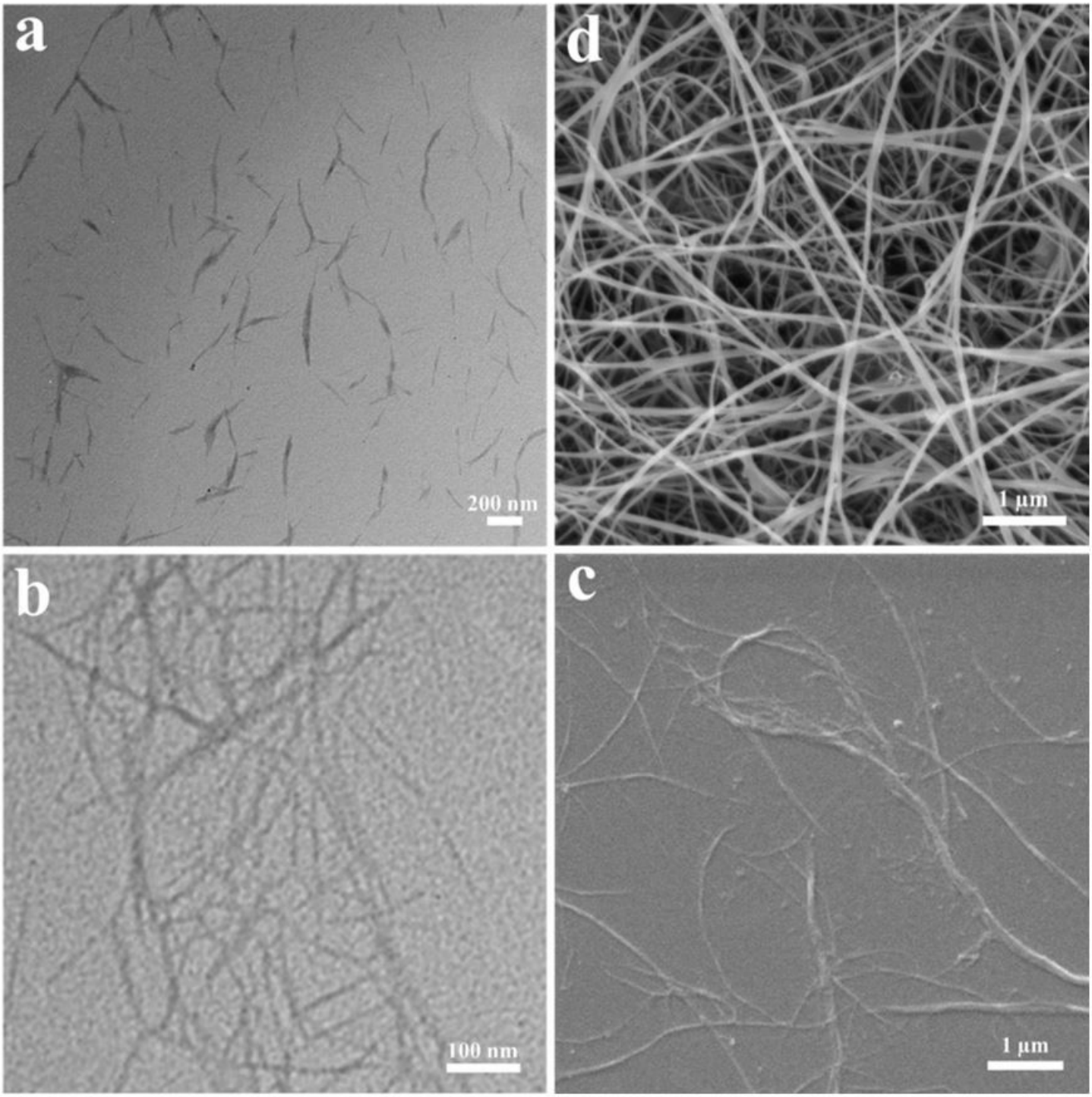

Figure 3

TEM images of nanocellulose. (a) sulfuric acid hydrolyzed CNC, (b) TEMPO oxidized CNF, (c) mechanically ground CNF, and (d) BC

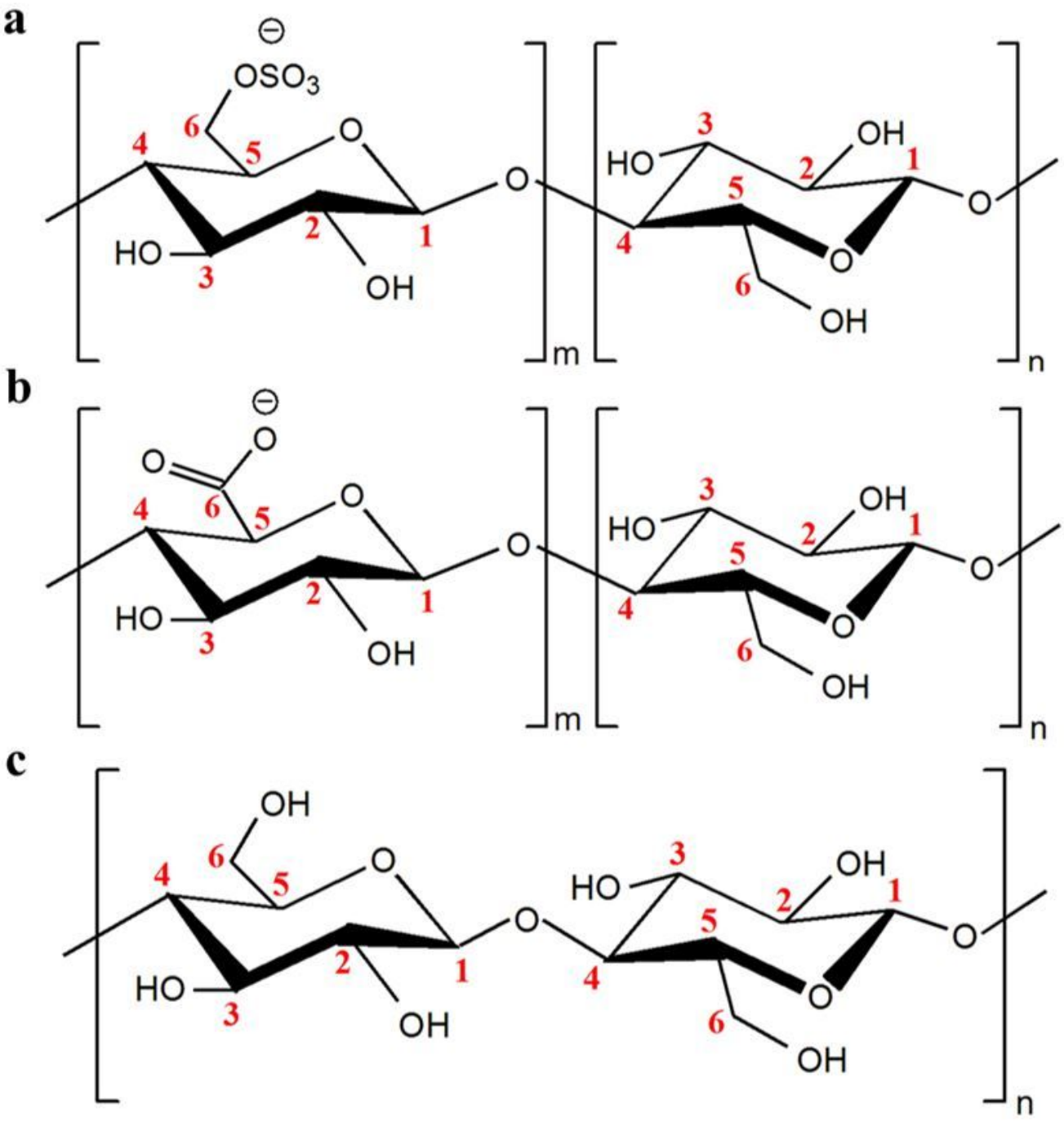

Figure 4

Chemical structure of nanocellulose. (a) sulfuric acid hydrolyzed CNC, (b) TEMPO oxidized CNF, and (c) mechanically ground CNF and BC (Sacui et al. 2014)

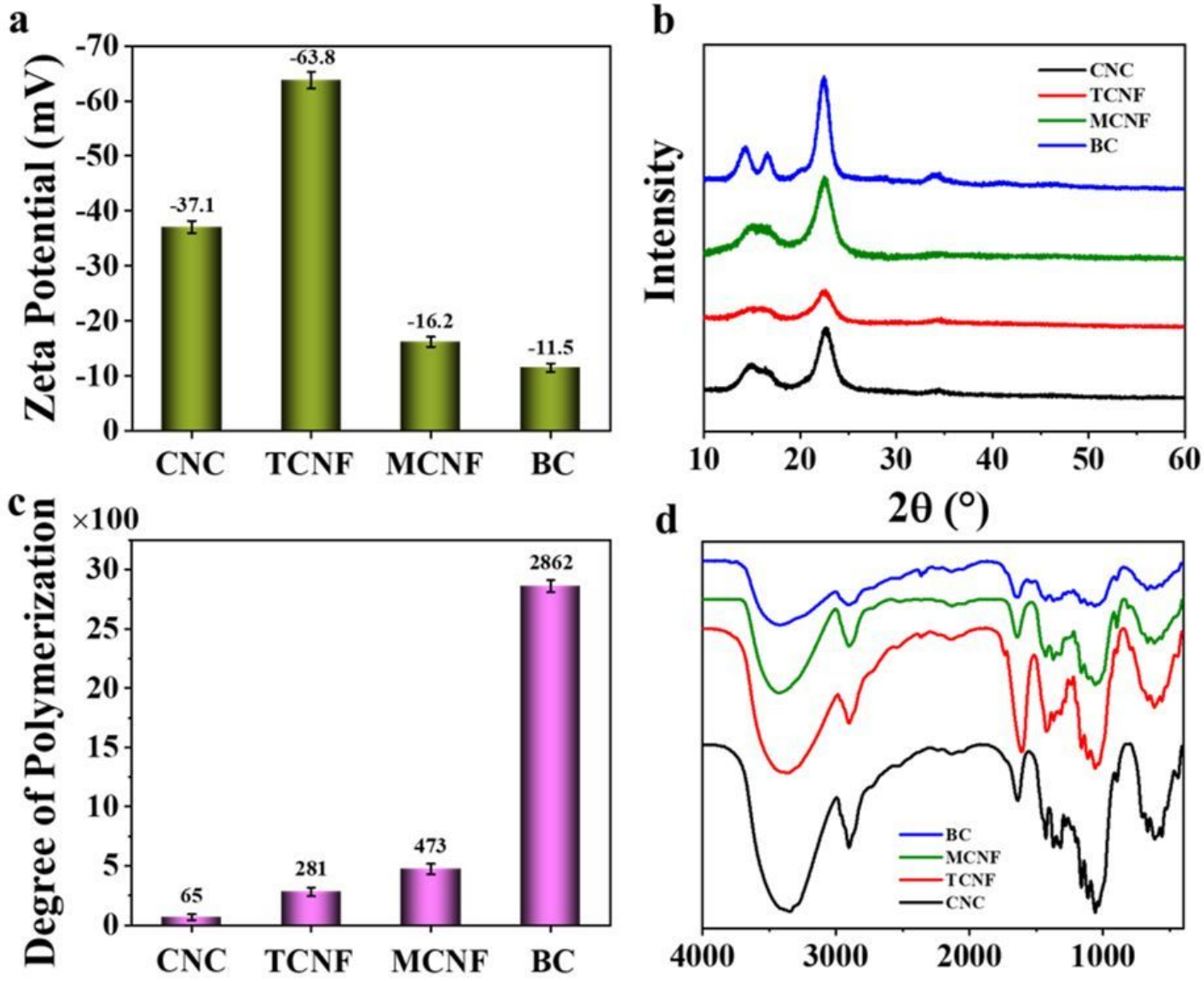

Figure 5

(a) Zeta potential, (b) XRD, (c) degree of polymerization, and (d) FTIR of sulfuric acid hydrolyzed CNC, TEMPO oxidized CNF, mechanically ground CNF, and BC

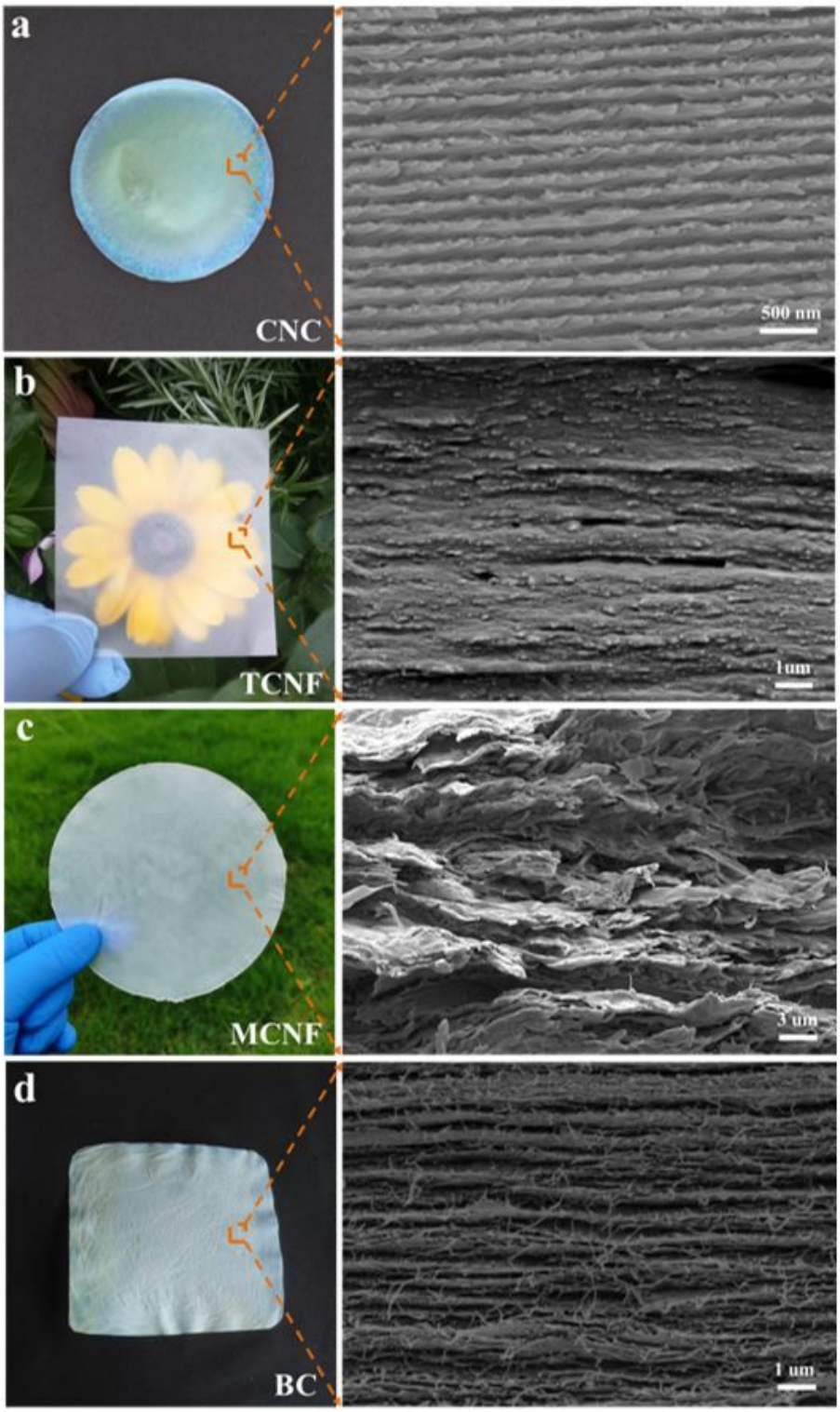

Figure 6

Photographs of solid nanocellulose films: (a) sulfuric acid hydrolyzed CNC, (b) TEMPO oxidized CNF, (c) mechanically ground CNF, and (d) BC

Figure 7

(a) Stress-strain curves, (b) Young’s modulus, (c) TG curves, and (d) DTG curves of sulfuric acid hydrolyzed CNC, TEMPO oxidized CNF, mechanically ground CNF, and BC, respectively